A Micro-Engineered Airway Lung-Chip Models Key Features of Viral-Induced Exacerbation of Asthma

Running title: Modeling human viral-induced asthma exacerbation on chip.

J. Nawroth[1§], C. Lucchesi[1§], D. Cheng[1], A. Shukla[1], J. Ngyuen[1], T. Shroff[1], K. Karalis[1], H-H. Lee[2], S. Alves[2], G. A. Hamilton[1*], M. Salmon[1,3], and R. Villenave[1*].

[1]Emulate, Inc., Boston, MA; [2]Merck Research Laboratories, Boston, MA; [3]formerly Merck Research Laboratories, Boston, MA

[§] Authors contributed equally to this work.

[*] Corresponding Authors: Remi Villenave, PhD, Roche, Basel CH-4070, Switzerland (ph: +41 79 759 04 52; email: remi.villenave@roche.com); Geraldine Hamilton, PhD, Emulate, Inc., Boston, MA (email: geraldine.hamilton@emulatebio.com).

At a Glance Commentary.

Scientific Knowledge on the Subject: New therapies for severe asthma, particularly treatments that reduce exacerbation, remain a significant unmet medical need. Development of human relevant preclinical models are needed to further elucidate the complex mechanisms underlying asthma exacerbation and investigate new therapeutic strategies.

What This Study Adds to the Field: Using a human Airway Lung-Chip model, we show here for the first time a live human rhinovirus (HRV) infection of the asthmatic epithelium that recapitulates complex clinical features of viral-induced asthma exacerbation. The dynamic microenvironment of the chip enables the real-time study of virus infection, epithelial response, and immune cell recruitment under healthy and asthmatic conditions. The model reproduces key endpoints that have been observed in asthmatics and individuals infected with rhinovirus including the ciliated cell sloughing, altered cilia beating frequency, goblet cells hyperplasia, increased expression of adhesion molecules in microvascular endothelial cells, and inflammatory mediator release. High-resolution temporal analysis of secreted inflammatory markers enabled by dynamic sampling revealed alteration of IL-6, IFN-λ1 and CXCL10 secretory phases after rhinovirus infection in an IL-13 high environment. Leveraging high-content imaging and analysis of circulating inflammatory cells, we demonstrated the efficacy of a CXCR2 antagonist to reduce adhesion, motility, and transmigration of perfused human neutrophils. Thus, this micro-engineered chip may offer a powerful addition to preclinical models for understanding mechanisms underlying asthma exacerbation pathology and developing new therapeutic strategies.

Abstract

Rationale: Viral-induced exacerbation of asthma are a major cause of hospitalization and mortality. Our understanding of the complex mechanisms underlying asthma exacerbation is hindered by the lack of physiological relevance and cellular complexity of traditional *in vitro* systems and the limited human translatability of animal models.

Objectives: To develop a new micro-engineered model of rhinovirus-induced asthma exacerbation that recapitulates live viral infection of asthmatic airway epithelium, neutrophil transepithelial migration, and enables evaluation of immunomodulatory therapy.

Methods: A micro-engineered model of fully differentiated human mucociliary airway epithelium was stimulated with IL-13 to induce a Th2-type asthmatic phenotype and infected with live human rhinovirus 16 (HRV16) to reproduce clinical features of viral-induced asthma exacerbation.

Measurements and Main Results: Infection with HRV16 replicated key hallmarks of the cytopathology and inflammatory responses observed in human airways. Generation of a Th2 microenvironment through exogenous IL-13 stimulation induced features of asthmatics airways, including goblet cell hyperplasia, reduction of cilia beating frequency, and endothelial activation, but did not alter rhinovirus infectivity or replication. High resolution kinetic analysis of secreted inflammatory markers revealed that IL-13 treatment altered the IL-6, IFN-λ1, and CXCL10 secretory phases in response to HRV16. Airway Lung-Chips perfused with human neutrophils demonstrated greatest neutrophil transepithelial migration when viral infection was combined with IL-13 treatment, while

treatment with MK-7123, a CXCR2 antagonist, reduced neutrophil diapedesis in all conditions.

Conclusions: This micro-engineered Airway Lung-Chip provides a novel human-relevant platform for exploring the complex mechanisms underlying viral-induced asthma exacerbation. Our data suggest that IL-13 may impair the hosts' ability to mount an appropriate and coordinated immune response to rhinovirus infection. We also show that the Airway Lung-Chip can be used to assess the efficacy of modulators of the immune response.

Key words: asthma exacerbation, rhinovirus, Organ-on-chip, Airway Lung-Chip, immune response, high-content imaging

Introduction.

Asthma is a highly prevalent chronic inflammatory disease of the respiratory tract defined by shortness of breath, wheezing, and chest tightness that affects 300 million people worldwide *(1)*. While significant therapeutic progress has been made in managing asthma with inhaled corticosteroids and bronchodilator medication, 5-10% of patients suffer from so-called severe asthma where the disease remains uncontrolled despite high-dose treatment, often resulting in exacerbation *(2)*. Asthma exacerbations are characterized by acute episodes of worsening asthma symptoms and decreased lung function that can lead to emergency hospitalizations and death. Indeed, the majority of morbidity, mortality and economic costs associated with asthma in developed countries derives from acute care for asthma exacerbations *(3, 4)*. Prevention and treatment of severe asthma attacks hence remains an area of considerable unmet medical need *(5)*. New human-relevant models that reproduce key aspects of the human physiology, function, and immune responses of the airways during exacerbation are critically needed in order to advance development of new therapeutics *(6)*.

Organs-on-chips offer the opportunity to generate physiologically relevant models of human tissue that recapitulate the multicellular architecture, tissue-tissue interfaces, physiochemical microenvironement (including mechanical forces such as shear stress), and vascular perfusion of the body *(7)*. Here, we have used an advanced microengineered Airway Lung-Chip that recapitulates the structure and function of a well-differentiated human mucociliary airway epithelium and its interaction with a continuously perfused microvascular pulmonary endothelium under physiological, *in vivo*-like haemodynamic shear stress *(8)* and applied it to generate a model of rhinovirus-induced

asthma exacerbation. Respiratory viral infections are believed to be a key trigger for exacerbations in children and adults, with human rhinovirus (HRV), a ubiquitous viral pathogen responsible for the common cold, being the most common infectious agent associated with exacerbations *(9)*. Respiratory viral infections trigger asthma exacerbation through several mechanisms, including airway inflammation, mucus hypersecretion, and bronchial hyperresponsiveness. Studies have also revealed association between impaired immune responses and asthma exacerbation during viral infection *(10, 11)*. The Airway Lung-Chip not only recapitulates many of these effects, but, in conjunction with innovative high-content imaging and microfluidic sampling strategies, it also provides new insights into how the asthmatic Th2 microenvironment derails the host immune responses. In addition, by allowing for the real-time evaluation of immune cell dynamics, the Airway Lung-Chip provides a novel platform for testing immunomodulatory therapeutics for the treatment and prevention of viral-induced asthma exacerbation.

Methods.

Complete methods can be found in the online supplement.

Cell differentiation and rhinovirus infection on-chip.

Cells were cultured and differentiated as previously described *(8)*. Briefly, hAECs were seeded in the Airway Lung-Chips on a human placenta collagen IV-coated 3-µm pore polyester membrane at a density of 3 x 10^6 cells/mL and left to attach for 2h. Five days post seeding, air liquid interface (ALI) was introduced and Airway Lung-Chips were

perfused basally at 60µL/h for 3 weeks until full differentiation. Epithelium integrity, ciliation, and apical mucus secretion were monitored for quality control. When complete epithelial differentiation was reached, hMVECs or HUVECs were seeded onto the opposite side of the membrane, in the vascular channel at a density of 1 x 10^7 cells/mL and cultured under flow for 3-4 days in endothelial growth media (EGM2-MV, Lonza, USA). Rhinovirus strain 16 (HRV-16) (ATCC® VR-283) was inoculated into the apical channel of fully differentiated Airway Lung-Chips and incubated for 3h at 33˚C while control chips received DMEM only. Following incubation, the epithelial channel of each chip was gently rinsed 5 x with DMEM. After the final wash, and every 24h thereafter, the epithelial surface was washed with 50 µL of DMEM to determine virus growth kinetics and the basolateral effluent was collected for cytokine/chemokine responses. HRV16 titers were determined by infecting H1-HeLa cells (CRL-1958) with serially diluted virus samples, recording the number of wells positive for viral CPE at each dilution after 5 days post infection and calculating the $TCID_{50}$/mL. A Th2 microenvironment was induced by perfusing Airway Lung-Chips with 100 ng/mL of IL-13 (Peprotech, USA) for 7 days. High-content imaging was performed in live and fixed tissues and followed by quantitative analysis to extract structural and kinematic endpoints, including ciliary beat frequency and neutrophil recruitment dynamics.

Results.

Generation of an on-chip model of the human airways that enables immune cell transmigration.

We developed a Lung Airway Lung-Chip suitable for the study of viral-induced asthma exacerbation and the effect of immunomodulatory compounds on immune cell dynamics. Here, we adapted our recently developed micro-engineered “small-airway-on-a-chip” model *(8)* and engineered a new chip design containing a membrane with increased pore size (3.0 µm vs 0.4 µm) to allow immune cells to transmigrate from the vascular microchannel to the epithelial lumen and thus replicate inflammatory infiltrates observed in exacerbations (**Fig. 1a**). To validate the new membrane configuration, human primary airway epithelial cells (hAECs) were cultured and differentiated at air liquid interface (ALI) for 21 days on top of the collagen-coated 3-µm pore membrane while differentiation medium was continuously perfused at 60 µL/h through the bottom channel. Human primary endothelial cells were then seeded on the opposite side of the membrane and cultured under similar flow rate until they became confluent to create a tissue-tissue interface (**Fig. 1a**).

Establishment of a well-differentiated mucociliary bronchiolar epithelium on one side of the 3-µm pore membrane and a confluent pulmonary microvascular endothelium on the opposite side was confirmed by immunofluorescence (**Fig. 1 b-f**). Robust Zo-1-containing tight junctions outlined a characteristic epithelial cobblestone-like morphology (**Fig. 1b**). MUC5AC staining revealed that ca. 18% of cell were mucus producing goblet cells and and β-tubulin staining identified ca. 30% of cells to be ciliated (**Fig. 1c, d**), which are proportions consistent with ranges found in normal human airways *(12)*. Immunostaining for the endothelial junctional protein VE-Cadherin showed the formation of an intact,

continuous microvascular endothelium opposed to the epithelium (**Fig. 1e**). Using high-speed, real-time microscopy, we found that cilia were actively beating in a synchronized fashion at a frequency of 16.35 (± 2.6) Hz (**Fig. 1f**, **g, Supplementary movie 1**), generating a locally unidirectional mucociliary transport visualized by recorded trajectories of rapidly moving fluorescent microbeads diluted in PBS and introduced in the top channel (**Fig. 1h**) as well as tumbling small plugs of cell debris trapped in mucus (**Supplementary movie 2**). The measured bead velocity was typically ~ 100 µm/sec, which is strikingly close to the values estimated for intact human airways *(13)*. Thus, the Airway Lung-Chip recapitulated key fundamental structural and functional parameters of normal human bronchioles suitable to investigate immune cells transmigration through its 3-µm pore membrane.

HRV16 readily infects the Airway Lung-Chip and induces cytopathic effects.

We next asked whether the Airway Lung-Chip model could also support infection of live respiratory virus and reproduce features of the cytopathic response observed *in vivo*. As human rhinovirus (HRV) is the pathogen most commonly associated with asthma exacerbation in adult and children *(9, 14)*, we infected the chip with HRV16, a rhinovirus serotype commonly used in clinical challenge studies, and analyzed viral infectivity and replication, cell tropism and induced cytopathic effects (CPE). Infection of the chips with HRV16 at a multiplicity of infection (MOI) of 1 resulted in a rapid apical release of infectious virus particles that peaked between 24 and 48 hours post infection (hpi) followed by a steady decline of released virions until no virus was detected 144 hpi (**Fig.**

2a), this timeframe was consistent with viral shedding and symptom score profiles of individuals experimentally infected with HRV *(15–17)*.

HRV16 readily infected the intact epithelium and induced significant apical cell sloughing by 24 hpi (**Fig. 2b**), indicative of a robust infection. Real time imaging and immunofluorescence characterization identified that the majority of detached cells were infected multiciliated cells (**Fig. 2c, Supplementary movie 3**), similar to what has been observed in respiratory tissue biopsies of human volunteers experimentally infected with HRV *(18, 19)*. Many of the detached cells were TUNEL-positive, indicating apoptosis (**Fig. 2d**). Immunofluorescence confocal microscopic analysis of infected chips revealed that HRV16 infection was restricted to ciliated cells and induced infected cells protrusion and extrusion from the epithelial lining, while mucus producing cells remained non-infected (**Fig.2 e, Supplementary movie 3**). By day 6 post infection, the majority of ciliated cells had disappeared from the epithelial surface (13 fold decrease cilia coverage; $p<0.001$) (**Fig. 2f, g**) while the few remaining ciliated cells displayed significantly shorter cilia (**Fig. 2f, Supplementary Fig. 1**). Interestingly, we found that not every ciliated cell was infected at 24 hpi, suggesting that several rounds of infection might occur during the course of infection. Additionally, consistent with HRV16 ciliated cells tropism, we observed a 60% reduction in cilia beating frequency following infection ($p<0.001$) (**Fig. 2h** and **Supplementary movie 4**). Furthermore, acute damage to ciliated cells was accompanied by a substantial epithelial remodeling characterized by a 2 x increase in the area covered by MUC5AC positive cells by 6 days post infection compared to non-infected control chips ($p<0.001$) (**Fig. 2i, j**), in line with previous clinical observation of human subjects infected with HRV *(20)*.

Modeling features of viral-induced asthma exacerbation on-chip.

To recapitulate HRV-induced asthma exacerbation in the Airway Lung-Chip and study the underlying mechanisms of the disease, we used interleukin-13 (IL-13) stimulation to induce features of Type 2 inflammation in asthma and combined this treatment with HRV16 infection to induce exacerbation (**Fig. 3a**). IL-13 plays a central role in allergic asthma and, together with IL-5, is an important mediator of viral-induced exacerbations in asthma *(21)*. When we treated the Airway Lung-Chip with IL-13 (100 ng/mL) for 7 days preceding virus infection, we detected a significant increase in the number of goblet cells (rising from 16.5% to 50.3% total area; $p<0.01$) (**Fig. 3b, c**) and a decrease in cilia beating frequency (14.4% reduction; $p<0.001$) (**Fig. 3d, e and Supplementary movie 5**), which is consistent with observations made in airway mucosa of asthmatic patients *(22, 23)*. When we infected the IL-13 treated Airway Lung-Chip with HRV16, we did not detect significant changes in viral loads in apical washes nor in the duration of infection when compared with non-stimulated chips (**Fig. 3f**). This finding was consistent with recent studies in adults and children asthmatics experimentally infected with HRV16 *(24–26)*.

Type 2 inflammation has been suggested to increase asthmatics susceptibility to exacerbations through airway remodeling and modulation of the antiviral response *(27)*. To gain insight into the effect of IL-13 on HRV16-induced inflammatory response we first measured the levels of pro-inflammatory cytokines and chemokines released apically and basolaterally at 24, 48 and 72 h post HRV16 infection, in the presence or absence of IL-13 (**Fig.4a-c and Supplementary Fig. 2**). Apical and basolateral secretion of CCL11, a potent eosinophil chemoattractant and markers of Th2 asthma in human *(28)*, was

increased following HRV16 infection (**Fig. 4a**). This was not significantly altered by IL-13 treatment. In contrast, apical secretion of CCL26, another chemokine associated with eosinophils recruitment and persistence in patients with asthma *(29)*, was increased at all time points following stimulation with IL-13 alone, while HRV16 infection had no effect on CCL26 release. Analysis of the interferon (IFN) type III response revealed that apical and basal release of IFN-λ1 at 48 hpi, and of IFN-induced lymphocytes chemoattractant CXCL10 at 48 and 72 hpi were increased following HRV16 infection (**Fig. 4b**). Markedly, IL-13 treatment significantly reduced measured IFN response in HRV16 infected chips, consistent with clinical reports showing that individuals with asthma or cells from asthmatics infected with HRV have a deficient IFN response *(30, 31)*, and supporting the idea that asthmatics have an impaired immune response to viral infections *(11)*. Furthermore, quantification of pro-inflammatory cytokines and chemokines associated with asthma exacerbations *in vivo* revealed increased IL-8 basal secretion 48 h post HRV16 infection and this was not significantly altered by IL-13 treatment (**Fig. 4c**). In contrast, we found that induction of IL-6 apical and basal secretion following HRV16 infection was greatly reduced in IL-13 treated samples at 48 h post infection (**Fig. 4c)**. Indeed, other studies have also found an altered cytokine expression in asthmatic airways in response to injury, potentially due to an altered proportion of basal cells relative to ciliated and goblet cells *(32)*. Notably, we did not detect any IFN-β secretion at any time point with and without IL-13 stimulation.

While measuring the level of secreted inflammatory mediators is essential to understand the nature and magnitude of the inflammatory response during exacerbation events, the kinetic profile of cytokines secretion is equally important to identify the distinct phases of

the pathophysiological process and investigate the mechanisms underlying the resolution of inflammation *(33, 34)*. To further elucidate the kinetics of inflammatory mediators release during viral-induced asthma exacerbations, we then leveraged the microperfusion of the Airway Lung-Chip for high resolution temporal profiling of IFN-λ1, CXCL10 and IL-6 secretion. By collecting basal medium flow-through every 2 h for 74h, we determined a temporal signature of IFN-λ1, CXCL10 and IL-6 secretory pattern, and identify distinct secretion phases (**Fig. 4d**). We found that IFN- λ1 increased exponentially until a peak at 22 h post HRV16 infection, followed by a plateau and a progressive decline to baseline level at 74 hpi. CXCL10 peaked later than IFN-λ1 at 34 h post infection, in line with CXCL10 direct interferon-dependent regulation. In contrast with the IFN response, we identified 4 distinct IL-6 kinetic phases, characterized by an immediate increase between 2 and 6 hpi, followed by a plateau, a rapid increase until 38 h post infection and a steady decline. High resolution profiling revealed clear statistically significant differences between IL-13-treated and non-treated cultures as early as 6 hpi ($p < 0.01$) for IL-6, and 8 hpi ($p < 0.05$) for IFN-λ1 and CXCL10 secretion ($p < 0.05$), while an IL-13 associated reduction was not detected in early (24 hpi) and late (72 hpi) daily media collection (**Fig.4b**), demonstrating that high resolution profiling is a more sensitive method for the detection of changes in cytokines release.

Complementing our understanding of the epithelial response, we also investigated the effect of IL-13 stimulation on human endothelial cells which, in combination with IL-8 secretion, initiates leukocyte recruitment and migration during asthma exacerbation. When we stimulated the Airway Lung-Chip through the vascular compartment with IL-13 (100 ng/mL) for 48 h, we observed progressive endothelium morphological changes

leading to the formation of cell aggregates throughout the vascular wall (**Fig. 5a**) accompanied by a 2 x increased endothelial cell density ($p < 0.0001$) (**Fig. 5b**). These morphological changes are in line with previous studies that indicate an involvement of the Interleukin-4 receptor (IL-4R) alpha chain (CD124) *(35)*. Analysis of genes expressed by endothelial cells cultured alone or under IL-13 stimulation (100 ng/mL) for 48 h showed upregulation of P-Selectin ($p = 0.036$) and E-Selectin ($p = 0.06$), two adhesion molecules involved in inflammatory cell recruitment (**Fig. 5c, Supplementary Table 2**). Fluorescence intensity of stained intercellular adhesion molecule 1 (ICAM-1) and vascular cell adhesion protein 1 (VCAM-1) was also significantly increased in IL-13 treated cultures compared to untreated control (**Fig. 5d, Supplementary Fig. 3**), supporting an active contribution of IL-13 to the inflammatory response and infiltration of immune cells through activation of the lung microvascular endothelium, in line with previous study showing increased adhesion molecules expression on endothelial cells in bronchial biopsies from subjects with asthma *(36)*.

Pharmacological modulation of neutrophil recruitment and transmigration by a CXCR2 antagonist on-chip.

While asthma is commonly associated with eosinophilia, neutrophils are the predominant cell type recovered from sputum during early stages of an acute asthma exacerbation *(37)*. When we perfused freshly isolated human neutrophils stained with a live dye through the lower channel of severe asthma chips under physiological flow and shear stress (1 dyn/cm^2), we observed neutrophil adhesion and crawling at the surface of the microvascular endothelium, rapidly followed by neutrophil transendothelial migration

through a combination of transcellular and paracellular migratory events (**Fig. 6a, b**). Treatment with IL-13 and HRV16, alone or in combination significantly increased neutrophil adhesion (**Fig. 6c, d**). Treatment with 10 μM MK-7123, a CXCR2 antagonist, at 24 hpi significantly reduced neutrophil adhesion to the endothelium induced by IL-13 and HRV16 alone or in combination by > 75% when compared with non-treated conditions (**Fig. 6c, d**). This response was accompanied by a reduction in neutrophil velocity (**Fig. 6e, f and Supplementary movies 6 and 7**). We also observed a significant twofold increase in neutrophil recruited between HRV infected chips and infected chips in presence of IL-13 (953 vs 1999; $p < 0.001$) (**Fig. 6d**).

Real time fluorescence imaging of circulating human neutrophils revealed that many endothelium bound neutrophils transmigrated from the vascular channel through the 3-μm pores of the membrane (which frequently merge into even larger pores in these track-etched membranes) into the epithelium channel where they adhered to the epithelial surface (**Fig. 6g and Supplementary movie 8**) and treatment with MK-7123 reduced the proportion of transmigrating neutrophils (**Fig. 6h**). Furthermore, characterization of fully migrated neutrophils revealed expression of myeloperoxidase (**Fig. 6i**), a marker of neutrophil activation found in lungs of asthmatics *(38)* that contributes to inflammation *in vivo (39)*. Thus, our on-chip disease model of asthma exacerbation not only enabled testing for the efficacy of an anti-inflammatory compound but also allowed further elucidation of the multi-step dynamics of neutrophil recruitment in a human-relevant context with the potential for clinical translation.

Discussion

We still incompletely understand why asthmatics are at higher risk of developing life-threatening exacerbation following rhinovirus infection. Previous *in vitro* studies have suggested that damage to the asthmatic airway epithelium induced by allergens or pollutants facilitates HRV infection by exposing more permissive, ICAM-1-expressing basal cells, explaining the inability of the asthmatic airway epithelium to effectively protect the lung from infection *(40, 41)*. The corollary is the perception that intact epithelial layers of healthy subjects are somewhat resistant to HRV infection, implying that HRV is generally non-cytopathic and unable to cause substantial damage to the epithelium *(42)*. Contrasting with this view, our findings demonstrate that HRV can readily infect the intact well-differentiated mucociliary epithelium on-chip and induce significant airway remodeling leading to almost complete loss of ciliated cells and goblet cell hyperplasia by day 7 post infection. More importantly, our observations are consistent with other studies showing high viral load and cell shedding in upper and lower airways of individuals infected with HRV *(18, 24–26)* and challenge the notion that a healthy airway epithelium is relatively resistant to HRV infection. Our data therefore suggest that HRV-induced CPE, including impaired mucociliary clearance and increased mucus production, contribute to exacerbations in asthmatic individuals and likely aggravate pre-existing tissue damage from chronic inflammatory conditions and epithelium remodeling from Th2 cytokines, such as IL-13.

Recognizing the central role of IL-13-induced epithelium remodeling in allergic asthma, several groups have investigated the effect of IL-13-induced mucous metaplasia on the susceptibility of human airway epithelium to HRV infection *(41, 43, 44)*. The studies,

however, have reported discordant findings. While one study showed that IL-13-induced mucous metaplasia increased susceptibility to HRV infection *(44)*, another one showed a reduced susceptibility of the airway epithelium to HRV infection *(43)*. In contrast, we did not detect any significant difference in viral load or infection persistence in IL-13 treated chips compared with non-treated controls. Difference in epithelial cells origin (tracheobronchial vs small airway), donor to donor variability, specific culture conditions (static vs dynamic) and/or infection protocols (incubation temperature and MOI) might explain the differences between previous reports and our data. However, our observations are supported by several recent clinical studies investigating viral load in asthmatics and non-asthmatics infected with HRV *(24–26, 45)*. Consistent with our results, these studies showed no difference in viral titer in both the upper and lower respiratory tracts of asthmatic and non-asthmatic, adults and children, infected with HRV. These studies serve to validate our findings and confirm the clinical relevance of the Airway Lung-Chip in modeling viral-induced asthma exacerbation.

Rather than an intrinsic susceptibility of asthmatics lungs to HRV infection, past studies have found that hAECs of asthmatics cultured *in vitro* displayed a deficient innate immunity to HRV infection *(11, 30, 31)*. We found that HRV-induced type III IFN response was ablated in a type 2 microenvironment, and these results were consistent with clinical studies showing impaired IFN response in asthmatic individuals challenged with HRV *(30, 46)*. However, several recent *in vitro* and *in vivo* studies have reported no difference in IFN signatures between asthmatics and non-asthmatic cells or individuals *(24, 26, 47, 48)*, demonstrating that HRV infections are often well controlled in asthmatics and suggesting that an impaired IFN responses may not be the only contributing factor to

initiate an exacerbation. These conflicting findings may be a consequence of asthma phenotype heterogeneity. It is possible that a deficient IFN response to HRV infection constitutes a distinct subset of asthma patients. In fact, an increased susceptibility to exacerbations through an impaired IFN response might be specific to asthmatics with a Th2-dominant inflammatory profile as studies and clinical trials for Th2 directed therapies seem to suggest *(21, 30)*, in line with our findings demonstrating the downregulation of IFN-λ1 by a Th2 microenvironment on chip.

Orchestration and resolution of the immune cell and tissue response relies on both magnitude and kinetics of secreted cytokines and chemokines. The pleiotropic inflammatory cytokine IL-6 is a prime example as its pro- or anti-inflammatory nature greatly depends on its secretion timing *(34)*. Here, we have leveraged the microscale perfusion of the Airway Lung-Chip to conduct high resolution profiling and reveal the release kinetics of inflammatory mediators. We found that IL-6 secretory phases are markedly disrupted by IL-13 stimulation. This could be due to the altered epithelial cell type composition of the asthmatic microenvironment, which, as we also show, induces goblet cell hyperplasia and other architectural changes *(49)*. The central role of IL-6 in infection and inflammation has been extensively described *(50)* and its protective role was highlighted in several studies. For instance, IL-6 has been shown to limit inflammation, promote protective adaptive immune response, and prevent fatal lung immunopathology induced by influenza virus infection *(51)*. IL-6 also plays a role in the resolution of innate immunity by contributing to the transition from the recruitment of neutrophils to lymphocytes and monocytes, thus helping prevent excessive tissue damage and promote repair *(33)*. IL-6 also tempers inflammatory responses by inducing

the secretion of anti-inflammatory IL-10 by T cells *(52)* and IL-6 overexpression in lungs of transgenic mice diminishes airway reactivity to methacholine *(53)* suggesting a role for IL-6 in airway homeostasis. More recently, a study in asthmatics and OVA sensitized mice infected with HRV showed that blocking of IL-25 receptor resulted in a reduction of the HRV-induced inflammatory response and cytokine expression, with the exception of IL-6, whose secretion increased in recovering animals *(54)*. Usually considered a pro-inflammatory mediator in asthma exacerbations, our results and others may suggest a more nuanced role for IL-6 in exacerbation pathogenesis.

One potential limitation of our platform is the incomplete repertoire of resident and immune cells present in asthmatic airways which can respond to the pro-and anti-inflammatory cues orchestrating the host immune response. However, a great advantage of our model system is the ability to independently modulate all the system parameters, including the inflammatory conditions, presence or absence of different cell types, and soluble factors to assess their relative contributions. For instance, while we focused on neutrophils due to their initial role in responding to HRV infection, in future work one could also systematically introduce other relevant cell types involved in asthma pathophysiology to study their individual contributions.

In summary, we developed a new on-chip human disease model of viral-induced asthma exacerbations that recapitulates hallmarks of rhinovirus-induced responses of the asthmatic airway. Owing to its unique fluidic design and accessibility to optical imaging, the Airway Lung-Chip also enables the high-resolution profiling of cytokine release, phenotypic changes and dynamic immune cell responses to immunomodulatory

therapies in a human-relevant context, thus adding a powerful pre-clinical platform for probing complex disease mechanisms and developing new treatments for severe asthma.

Acknowledgments.

We thank Dr. Anne van der Does and Dr. Gurpreet Brar for the critical review of the manuscript and Brett Clair for his assistance with graphic design.

Declaration of Interests.

C.L., J.N., A.S., J.N., K.K., T.S, G. H, and R.V. are employees and hold equity of Emulate, Inc.

References.

1. M. Masoli, D. Fabian, S. Holt, R. Beasley, Global Initiative for Asthma (GINA) Program, The global burden of asthma: executive summary of the GINA Dissemination Committee report., *Allergy* **59**, 469–78 (2004).

2. M. R. Sears, Trends in the Prevalence of Asthma, , 219–225 (2014).

3. L. Watson, F. Turk, P. James, S. T. Holgate, Factors associated with mortality after an asthma admission: A national United Kingdom database analysis, *Respir. Med.* **101**, 1659–1664 (2007).

4. K. Smith, T. Warholak, E. Armstrong, M. Leib, R. Rehfeld, D. Malone, Evaluation of

Risk Factors and Health Outcomes among Persons with Asthma, *J. Asthma* **46**, 234–237 (2009).

5. J. R. Castillo, S. P. Peters, W. W. Busse, Asthma Exacerbations: Pathogenesis, Prevention, and Treatment., *J. allergy Clin. Immunol. Pract.* **5**, 918–927 (2016).

6. A. M. Holmes, R. Solari, S. T. Holgate, Animal models of asthma: value, limitations and opportunities for alternative approaches., *Drug Discov. Today* **16**, 659–70 (2011).

7. S. N. Bhatia, D. E. Ingber, Microfluidic organs-on-chips., *Nat. Biotechnol.* **32**, 760–772 (2014).

8. K. H. Benam, R. Villenave, C. Lucchesi, A. Varone, C. Hubeau, H.-H. Lee, S. E. Alves, M. Salmon, T. C. Ferrante, J. C. Weaver, A. Bahinski, G. A. Hamilton, D. E. Ingber, Small airway-on-a-chip enables analysis of human lung inflammation and drug responses in vitro., *Nat. Methods* **13**, 151–7 (2016).

9. D. J. Jackson, S. L. Johnston, The role of viruses in acute exacerbations of asthma., *J. Allergy Clin. Immunol.* **125**, 1178–87; quiz 1188–9 (2010).

10. M. Contoli, S. D. Message, V. Laza-Stanca, M. R. Edwards, P. a B. Wark, N. W. Bartlett, T. Kebadze, P. Mallia, L. A. Stanciu, H. L. Parker, L. Slater, A. Lewis-Antes, O. M. Kon, S. T. Holgate, D. E. Davies, S. V Kotenko, A. Papi, S. L. Johnston, Role of deficient type III interferon-lambda production in asthma exacerbations., *Nat. Med.* **12**, 1023–6 (2006).

11. P. A. B. Wark, S. L. Johnston, F. Bucchieri, R. Powell, S. Puddicombe, V. Laza-Stanca, S. T. Holgate, D. E. Davies, Asthmatic bronchial epithelial cells have a deficient

innate immune response to infection with rhinovirus., *J. Exp. Med.* **201**, 937–47 (2005).

12. R. R. Mercer, M. L. Russell, V. L. Roggli, J. D. Crapo, Cell number and distribution in human and rat airways., *Am. J. Respir. Cell Mol. Biol.* **10**, 613–24 (1994).

13. W. Hofmann, B. Asgharian, Comparison of Mucociliary Clearance Velocities in Human and Rat Lungs for Extrapolation Modeling, **46**, 323–325 (2002).

14. S. L. Johnston, P. K. Pattemore, G. Sanderson, S. Smith, F. Lampe, L. Josephs, P. Symington, S. O'Toole, S. H. Myint, D. a Tyrrell, Community study of role of viral infections in exacerbations of asthma in 9-11 year old children., *BMJ* **310**, 1225–1229 (1995).

15. F. G. Hayden, G. J. Hipskind, D. H. Woerner, G. F. Eisen, M. Janssens, P. A. J. Janssen, K. Andries, Intranasal pirodavir (R77,975) treatment of rhinovirus colds, *Antimicrob. Agents Chemother.* **39**, 290–294 (1995).

16. J. E. Gern, A. G. Mosser, C. A. Swenson, P. J. Rennie, R. J. England, J. Shaffer, H. Mizoguchi, Inhibition of rhinovirus replication in vitro and in vivo by acid-buffered saline., *J. Infect. Dis.* **195**, 1137–1143 (2007).

17. Y. Igarashi, D. P. Skoner, W. J. Doyle, M. V. White, P. Fireman, M. A. Kaliner, Analysis of nasal secretions during experimental rhinovirus upper respiratory infections, *J. Allergy Clin. Immunol.* **92**, 722–731 (1993).

18. R. B. Tumer, J. O. Hendley, J. M. Gwaltney, Shedding of infected ciliated epithelial cells in rhinovirus colds, *J. Infect. Dis.* **145**, 849–853 (1982).

19. A. G. Mosser, R. Vrtis, L. Burchell, W. M. Lee, C. R. Dick, E. Weisshaar, D. Bock, C.

A. Swenson, R. D. Cornwell, K. C. Meyer, N. N. Jarjour, W. W. Busse, J. E. Gern, Quantitative and qualitative analysis of rhinovirus infection in bronchial tissues, *Am. J. Respir. Crit. Care Med.* **171**, 645–651 (2005).

20. C. A. Hewson, J. J. Haas, N. W. Bartlett, S. D. Message, V. Laza-Stanca, T. Kebadze, G. Caramori, J. Zhue, M. R. Edbrooke, L. A. Stanciu, O. M. Kon, A. Papi, P. K. Jefferye, M. R. Edwards, S. L. Johnston, Rhinovirus induces MUC5AC in a human infection model and in vitro via NF-κB and EGFR pathways, *Eur. Respir. J.* **36**, 1425–1435 (2010).

21. J. V Fahy, Type 2 inflammation in asthma--present in most, absent in many., *Nat. Rev. Immunol.* **15**, 57–65 (2015).

22. B. Thomas, A. Rutman, R. A. Hirst, P. Haldar, A. J. Wardlaw, J. Bankart, C. E. Brightling, C. O'Callaghan, Ciliary dysfunction and ultrastructural abnormalities are features of severe asthma., *J. Allergy Clin. Immunol.* **126**, 722-729.e2 (2010).

23. C. L. Ordoñez, R. Khashayar, H. H. Wong, R. Ferrando, R. Wu, D. M. Hyde, J. A. Hotchkiss, Y. Zhang, A. Novikov, G. Dolganov, J. V Fahy, Mild and moderate asthma is associated with airway goblet cell hyperplasia and abnormalities in mucin gene expression., *Am. J. Respir. Crit. Care Med.* **163**, 517–23 (2001).

24. J. L. Kennedy, M. Shaker, V. McMeen, J. Gern, H. Carper, D. Murphy, W. M. Lee, Y. A. Bochkov, R. F. Vrtis, T. Platts-Mills, J. Patrie, L. Borish, J. W. Steinke, W. A. Woods, P. W. Heymann, Comparison of viral load in individuals with and without asthma during infections with rhinovirus, *Am. J. Respir. Crit. Care Med.* **189**, 532–539 (2014).

25. L. C. Denlinger, R. L. Sorkness, W.-M. Lee, M. D. Evans, M. J. Wolff, S. K. Mathur, G. M. Crisafi, K. L. Gaworski, T. E. Pappas, R. F. Vrtis, E. A. Kelly, J. E. Gern, N. N. Jarjour, Lower airway rhinovirus burden and the seasonal risk of asthma exacerbation., *Am. J. Respir. Crit. Care Med.* **184**, 1007–14 (2011).

26. J. P. DeMore, E. H. Weisshaar, R. F. Vrtis, C. A. Swenson, M. D. Evans, A. Morin, E. Hazel, J. A. Bork, S. Kakumanu, R. Sorkness, W. W. Busse, J. E. Gern, Similar colds in subjects with allergic asthma and nonatopic subjects after inoculation with rhinovirus-16., *J. Allergy Clin. Immunol.* **124**, 245–52, 252.e1–3 (2009).

27. E. M. Dunican, J. V Fahy, The Role of Type 2 Inflammation in the Pathogenesis of Asthma Exacerbations., *Ann. Am. Thorac. Soc.* **12 Suppl 2**, S144-9 (2015).

28. D. Wu, J. Zhou, H. Bi, L. Li, W. Gao, M. Huang, I. M. Adcock, P. J. Barnes, X. Yao, CCL11 as a potential diagnostic marker for asthma?, *J. Asthma* **51**, 847–854 (2014).

29. A. J. Ravensberg, F. L. M. Ricciardolo, A. Van Schadewijk, K. F. Rabe, P. J. Sterk, P. S. Hiemstra, T. Mauad, Eotaxin-2 and eotaxin-3 expression is associated with persistent eosinophilic bronchial inflammation in patients with asthma after allergen challenge, *J. Allergy Clin. Immunol.* **115**, 779–785 (2005).

30. S. Baraldo, M. Contoli, E. Bazzan, G. Turato, A. Padovani, B. Marku, F. Calabrese, G. Caramori, A. Ballarin, D. Snijders, A. Barbato, M. Saetta, A. Papi, Deficient antiviral immune responses in childhood: distinct roles of atopy and asthma., *J. Allergy Clin. Immunol.* **130**, 1307–14 (2012).

31. M. Contoli, S. Message, V. Laza-Stanca, Role of deficient type III interferon-λ production in asthma exacerbations. Supplements, *Nat. Med.* **1** (2006) (available at

http://www.nature.com/nm/journal/v12/n9/abs/nm1462.html).

32. B. Xie, B. Laxman, S. Hashemifar, R. Stern, C. Gilliam, N. Maltsev, S. R. White, Chemokine expression in the early response to injury in human airway epithelial cells, , 1–22 (2018).

33. S. A. Jones, Directing transition from innate to acquired immunity: defining a role for IL-6, *J. Immunol. (Baltimore, Md. 1950)* **175**, 3463–3468 (2005).

34. C. J. Pyle, F. I. Uwadiae, D. P. Swieboda, J. A. Harker, Early IL-6 signalling promotes IL-27 dependent maturation of regulatory T cells in the lungs and resolution of viral immunopathology, *PLoS Pathog.* **13**, 1–27 (2017).

35. K. Kotowicz, R. E. Callard, K. Friedrich, D. J. Matthews, N. Klein, Biological activity of IL-4 and IL-13 on human endothelial cells: functional evidence that both cytokines act through the same receptor, *Int Immunol* **8**, 1915–1925 (1996).

36. Y. Ohkawara, K. Yamauchi, N. Maruyama, H. Hoshi, I. Ohno, M. Honma, Y. Tanno, G. Tamura, K. Shirato, H. Ohtani, In situ expression of the cell adhesion molecules in bronchial tissues from asthmatics with air flow limitation: in vivo evidence of VCAM-1/VLA-4 interaction in selective eosinophil infiltration., *Am. J. Respir. Cell Mol. Biol.* **12**, 4–12 (1995).

37. J. V Fahy, Eosinophilic and neutrophilic inflammation in asthma: insights from clinical studies., *Proc. Am. Thorac. Soc.* **6**, 256–9 (2009).

38. A. JATAKANON, C. UASUF, W. MAZIAK, S. LIM, K. F. CHUNG, P. J. BARNES, Neutrophilic Inflammation in Severe Persistent Asthma, *Am. J. Respir. Crit. Care Med.*

160, 1532–1539 (1999).

39. E. Kolaczkowska, P. Kubes, Neutrophil recruitment and function in health and inflammation., *Nat. Rev. Immunol.* **13**, 159–75 (2013).

40. U. Sajjan, Q. Wang, Y. Zhao, D. C. Gruenert, M. B. Hershenson, Rhinovirus disrupts the barrier function of polarized airway epithelial cells, *Am. J. Respir. Crit. Care Med.* **178**, 1271–1281 (2008).

41. N. Lopez-Souza, G. Dolganov, R. Dubin, L. A. Sachs, L. Sassina, H. Sporer, S. Yagi, D. Schnurr, H. A. Boushey, J. H. Widdicombe, Resistance of differentiated human airway epithelium to infection by rhinovirus., *Am. J. Physiol. Lung Cell. Mol. Physiol.* **286**, L373–L381 (2004).

42. J. E. Gern, The ABCs of rhinoviruses, wheezing, and asthma., *J. Virol.* **84**, 7418–26 (2010).

43. B. Jakiela, A. Gielicz, H. Plutecka, M. Hubalewska-Mazgaj, L. Mastalerz, G. Bochenek, J. Soja, R. Januszek, A. Aab, J. Musial, M. Akdis, C. A. Akdis, M. Sanak, Th2-type cytokine-induced mucus metaplasia decreases susceptibility of human bronchial epithelium to rhinovirus infection, *Am. J. Respir. Cell Mol. Biol.* **51**, 229–241 (2014).

44. M. E. Lachowicz-Scroggins, H. A. Boushey, W. E. Finkbeiner, J. H. Widdicombe, Interleukin-13-induced mucous metaplasia increases susceptibility of human airway epithelium to rhinovirus infection., *Am. J. Respir. Cell Mol. Biol.* **43**, 652–61 (2010).

45. H. E. Fleming, F. F. Little, D. Schnurr, P. C. Avila, H. Wong, J. Liu, S. Yagi, H. A.

Boushey, Rhinovirus-16 colds in healthy and in asthmatic subjects: Similar changes in upper and lower airways, *Am. J. Respir. Crit. Care Med.* **160**, 100–108 (1999).

46. T. T. Hansel, T. Tunstall, M. Trujillo-torralbo, B. Shamji, A. Telcian, J. Aniscenko, L. Gogsadze, E. Bakhsoliani, L. Stanciu, N. Bartlett, M. Edwards, R. Walton, P. Mallia, T. M. Hunt, T. L. Hunt, D. G. Hunt, J. Westwick, M. Edwards, O. Min, D. J. Jackson, S. L. Johnston, EBioMedicine A Comprehensive Evaluation of Nasal and Bronchial Cytokines and Chemokines Following Experimental Rhinovirus Infection in Allergic Asthma : Increased Interferons (IFN- γ and IFN- λ) and Type 2 In fl ammation (IL-5 and IL-13), *EBioMedicine* **19**, 128–138 (2017).

47. Y. A. Bochkov, K. M. Hanson, S. Keles, R. A. Brockman-schneider, N. N. Jarjour, Rhinovirus-induced modulation of gene expression in bronchial epithelial cells from subjects with asthma, *Mucosal Immunol.* **3**, 69–80 (2010).

48. N. Lopez-Souza, S. Favoreto, H. Wong, T. Ward, S. Yagi, D. Schnurr, W. E. Finkbeiner, G. M. Dolganov, J. H. Widdicombe, H. A. Boushey, P. C. Avila, In vitro susceptibility to rhinovirus infection is greater for bronchial than for nasal airway epithelial cells in human subjects., *J. Allergy Clin. Immunol.* **123**, 1384–90.e2 (2009).

49. M. A. Seibold, Interleukin-13 Stimulation Reveals the Cellular and Functional Plasticity of the Airway Epithelium, **15** (2018), doi:10.1513/AnnalsATS.201711-868MG.

50. C. A. Hunter, S. A. Jones, IL-6 as a keystone cytokine in health and disease., *Nat. Immunol.* **16**, 448–57 (2015).

51. S. N. Lauder, E. Jones, K. Smart, A. Bloom, A. S. Williams, J. P. Hindley, B. Ondondo, P. R. Taylor, M. Clement, C. Fielding, A. J. Godkin, S. A. Jones, A. M.

Gallimore, Interleukin-6 limits influenza-induced inflammation and protects against fatal lung pathology, *Eur. J. Immunol.* **43**, 2613–2625 (2013).

52. J. S. Stumhofer, J. S. Silver, A. Laurence, P. M. Porrett, T. H. Harris, L. A. Turka, M. Ernst, C. J. M. Saris, J. J. O'Shea, C. A. Hunter, Interleukins 27 and 6 induce STAT3-mediated T cell production of interleukin 10., *Nat. Immunol.* **8**, 1363–1371 (2007).

53. B. F. DiCosmo, G. P. Geba, D. Picarella, J. A. Elias, J. A. Rankin, B. R. Stripp, J. A. Whitsett, R. A. Flavell, Airway epithelial cell expression of interleukin-6 in transgenic mice. Uncoupling of airway inflammation and bronchial hyperreactivity., *J. Clin. Invest.* **94**, 2028–35 (1994).

54. J. Beale, A. Jayaraman, D. J. Jackson, J. D. R. Macintyre, M. R. Edwards, R. P. Walton, J. Zhu, Y. Man Ching, B. Shamji, M. Edwards, J. Westwick, D. J. Cousins, Y. Yi Hwang, A. McKenzie, S. L. Johnston, N. W. Bartlett, Rhinovirus-induced IL-25 in asthma exacerbation drives type 2 immunity and allergic pulmonary inflammation., *Sci. Transl. Med.* **6**, 256ra134 (2014).

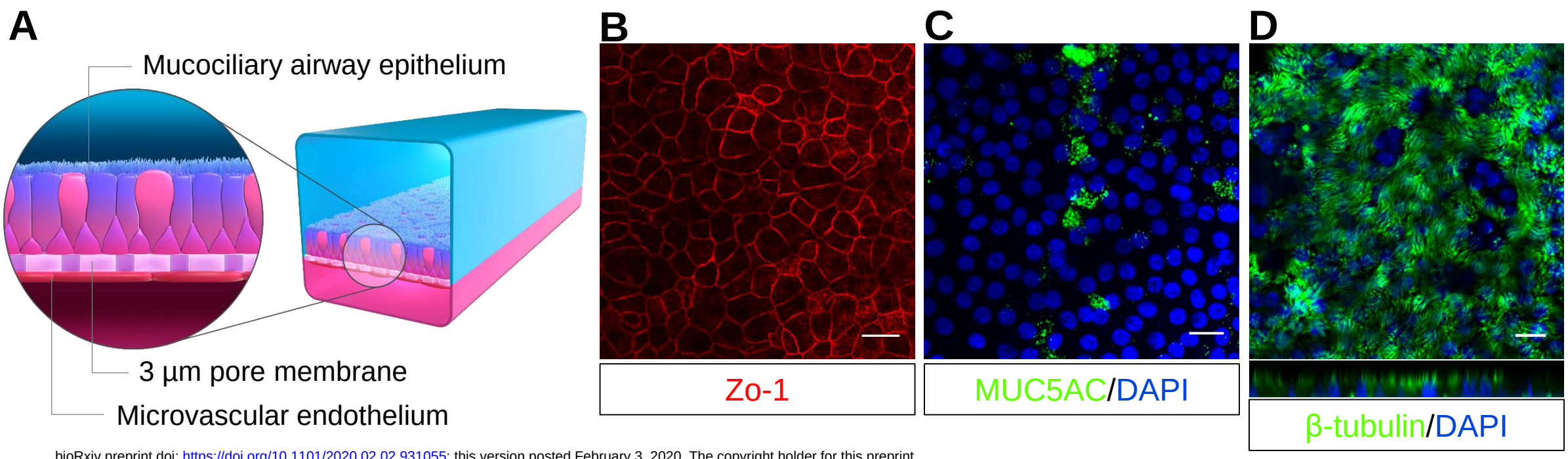

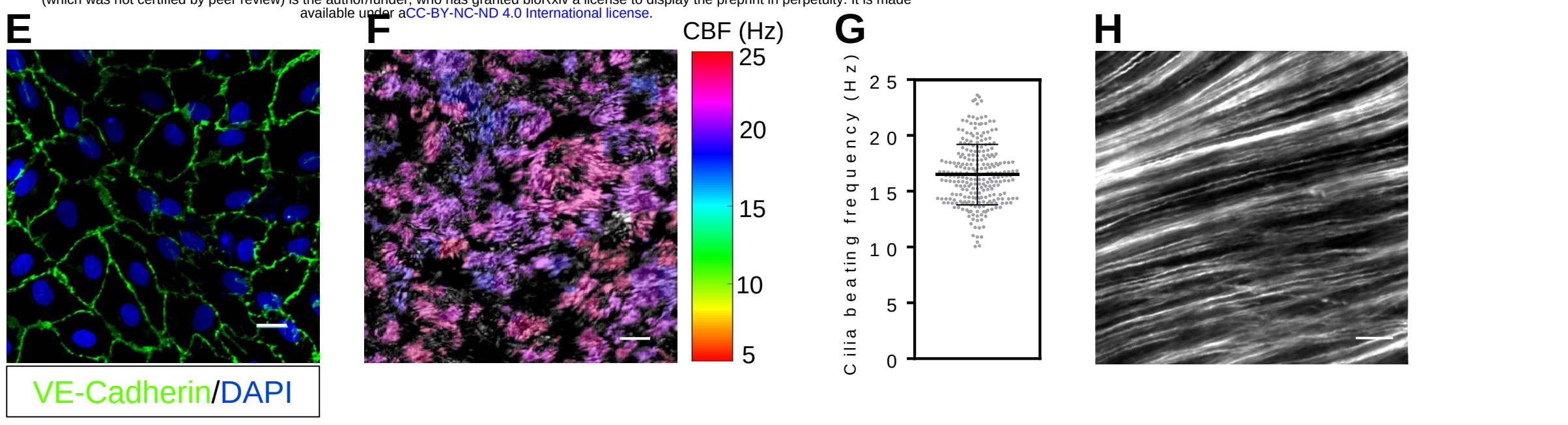

Fig 1. The human Airway chip. (**A**) Schematic diagram of the human Airway chip with a 3µm pore PET membrane. (**B**) The differentiated airway epithelium exhibits continuous tight junctional connections on-chip, as demonstrated by Zo-1 staining (red). Scale bar, 20 µm. (**C-D**) The well-differentiated human airway epithelium generated on-chip also contains goblet cells stained for MUC5AC (green) and demonstrates extensive coverage of ciliated cells labelled for β-tubulin (green). Scale bar, 20 µm. (**E**) The human (lung blood microvascular) endothelial monolayer formed on-chip contained continuous adherens junctions between adjacent cells, as indicated by VE-Cadherin staining (green). Scale bar, 10 µm. All images are representative of two to five independent experiments performed with cells from three different donors. (**F**) Graphic representation of cilia beating frequency (CBF) on-chip generated from a high speed recording of cilia beating in a representative field of view. Scale shows color coded CBF values in Hz. Scale bar, 20 µm. (**G**) The graph shows the cilia beating frequency measured in 5-10 random on-chip fields of view and each dot represents regions of ciliary beating. Data have been recorded in cells from three different donors and are presented as mean ± SD. (**H**) Composite real time micrograph of a 5 sec recording of fluorescent microbeads path lines at the surface of the epithelium revealing the mucociliary activity of the differentiated hAECs. Scale bar, 20 µm.

FIGURE 1

Fig 2. **HRV-16 infects the airway chip and induces cytopathic effects**. (**A**) The graph shows the viral growth kinetic of HRV-16 following infection of the airway chip at an MOI~1. HRV16 was titrated in apical washes and data represent mean ± SD log10 $TCID_{50}$/ml from 3 different donors with two to five biological replicates per donor. The dashed line indicate the limit of detection of the titration assay. (**B**) Bright field micrographs of differentiated airway epithelium cultured in the airway chip for 3 weeks at air liquid interface infected with HRV16 for 24h (right) or non infected (left) showing epithelial cells sloughed off infected cultures while non infected epithelium remains intact. Scale bar, 50 µm (applies to both views). (**C**) Immunofluorescence confocal micrographic view of apical washes from cultures infected with HRV16 for 24h showing detached cells stained for β-tubulin (green), mAbJ2 (red) and DAPI (blue). Scale bar, 10 µm. (**D**) Fluorescence confocal micrograph of detached epithelial cells stained using the TUNEL assay showing nuclei of apoptotic (green) and non apoptotic (blue) cells. Scale bar, 20 µm. (**E**) Immunofluorescence confocal micrograph of the differentiated mucociliary epithelium on-chip infected with HRV16 for 24h and stained for β-tubulin (left) or MUC5AC (right) (green) and mAbJ2 (red). Orthogonal views show a ciliated infected cells protruding from the epithelial lining (white arrow). Scale bar, 20 µm. (**F**) Immunofluorescence images of the differentiated epithelium non infected (left) or fixed at 6 days post HRV16 infection (right) and stained for β-tubulin (green) and DAPI (blue). Scale bar, 20 µm. (**G**) Total culture area covered by ciliated cells in non infected chips and 6 days post HRV16 infection. (**H**) Cilia beating frequency in non infected chips and 72 hpi. (**I**) Immunofluorescence images of the differentiated epithelium non infected (left) or 6 days post HRV16 infection (right) and stained for MUC5AC (red) and DAPI (blue). Scale bar, 20 µm. (**J**) Total culture area covered by goblet cells in non infected control and HRV16 infected chips 6 dpi. Data are from chips with cells from three healthy donors, with one or two biological replicates (chips) per donor. Data represent mean ±SEM and significance was determined by unpaired Student's; ****P < 0.0001.

FIGURE 2

Fig 3. Modeling HRV-induced asthma exacerbation on chip. (**A**) The severe asthma chip was generated by inducing features of Th2 asthma through vascular perfusion of IL-13 (100 ng/mL) and exacerbation through HRV16 epithelial infection (MOI 1). (**B**) Immunofluorescence confocal views of differentiated airway epithelium cultured at air-liquid interface for 3 weeks on-chip in the absence (left) or presence (right) of IL-13 (100 ng/mL) for 7 days showing epithelium stained for the goblet cell marker MUC5AC (green) and nuclei (blue). Scale bar, 20 µm (applies to both views); images are representative of two independent experiments performed on cells from three different donors. (**C**) Total culture area covered by goblet cells in absence or presence of IL-13 (100 ng/mL) for 7 days. (**D**) Heat map of cilia beating frequency (CBF) on-chip generated from a high speed recording of cilia beating in a representative field of view in absence or presence of IL-13 (100 ng/mL). Scale shows color coded CBF values in Hz. Scale bar, 20 µm. (**E**) Graph showing Cilia beating frequency in absence or presence of IL-13 (100 ng/mL). Data represent mean ±SEM and significance was determined by unpaired Student's; ***P < 0.001, ****P < 0.0001. (**F**) This graph shows the viral growth kinetic of HRV-16 following infection of the airway chip at an MOI~1 in the absence or presence of IL-13. HRV-16 was titrated in apical washes and data represent mean ± SD log10 $TCID_{50}$/ml from 3 different donors with two to five biological replicates per donor.

FIGURE 3

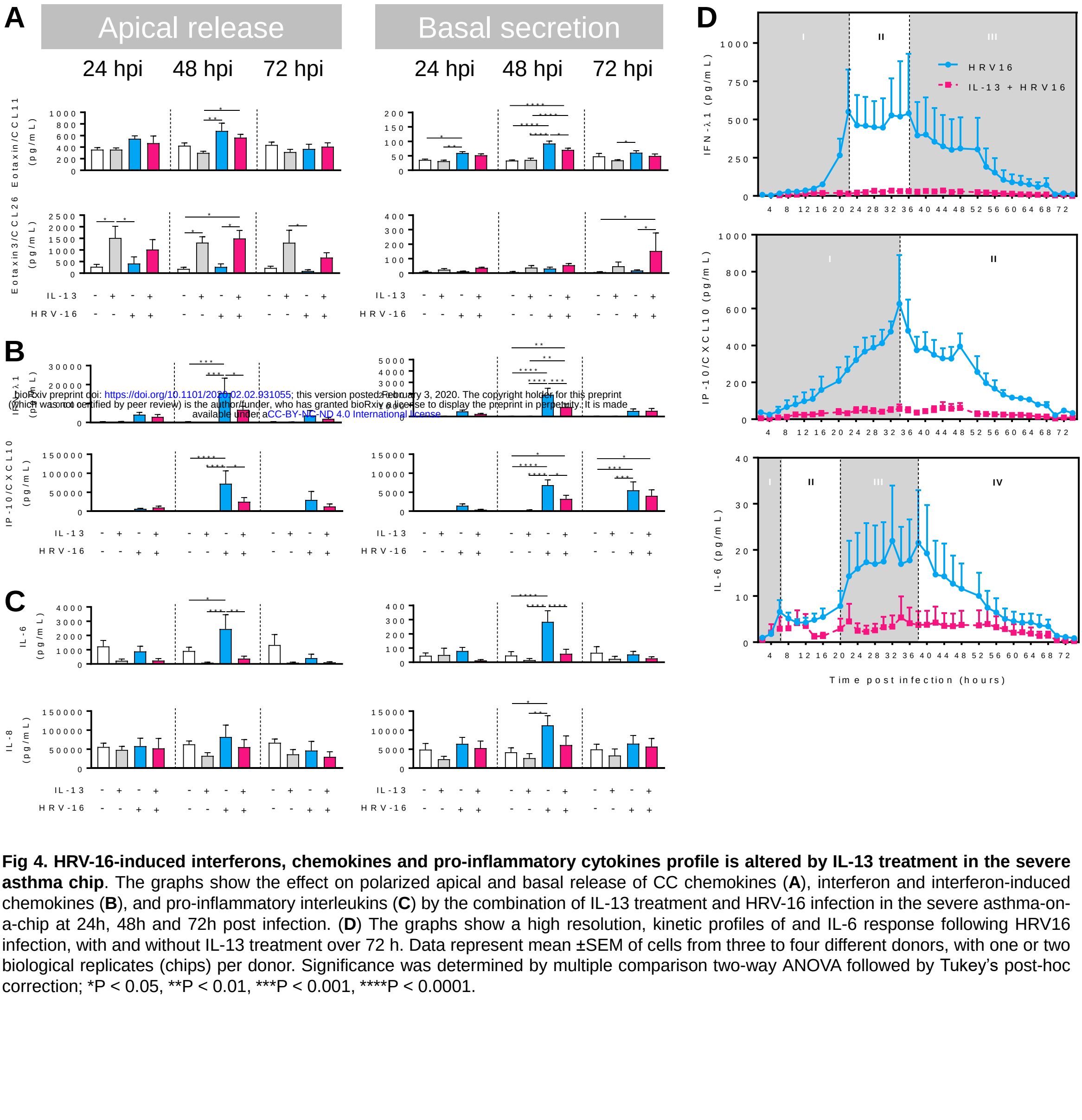

Fig 4. HRV-16-induced interferons, chemokines and pro-inflammatory cytokines profile is altered by IL-13 treatment in the severe asthma chip. The graphs show the effect on polarized apical and basal release of CC chemokines (**A**), interferon and interferon-induced chemokines (**B**), and pro-inflammatory interleukins (**C**) by the combination of IL-13 treatment and HRV-16 infection in the severe asthma-on-a-chip at 24h, 48h and 72h post infection. (**D**) The graphs show a high resolution, kinetic profiles of and IL-6 response following HRV16 infection, with and without IL-13 treatment over 72 h. Data represent mean ±SEM of cells from three to four different donors, with one or two biological replicates (chips) per donor. Significance was determined by multiple comparison two-way ANOVA followed by Tukey's post-hoc correction; *P < 0.05, **P < 0.01, ***P < 0.001, ****P < 0.0001.

FIGURE 4

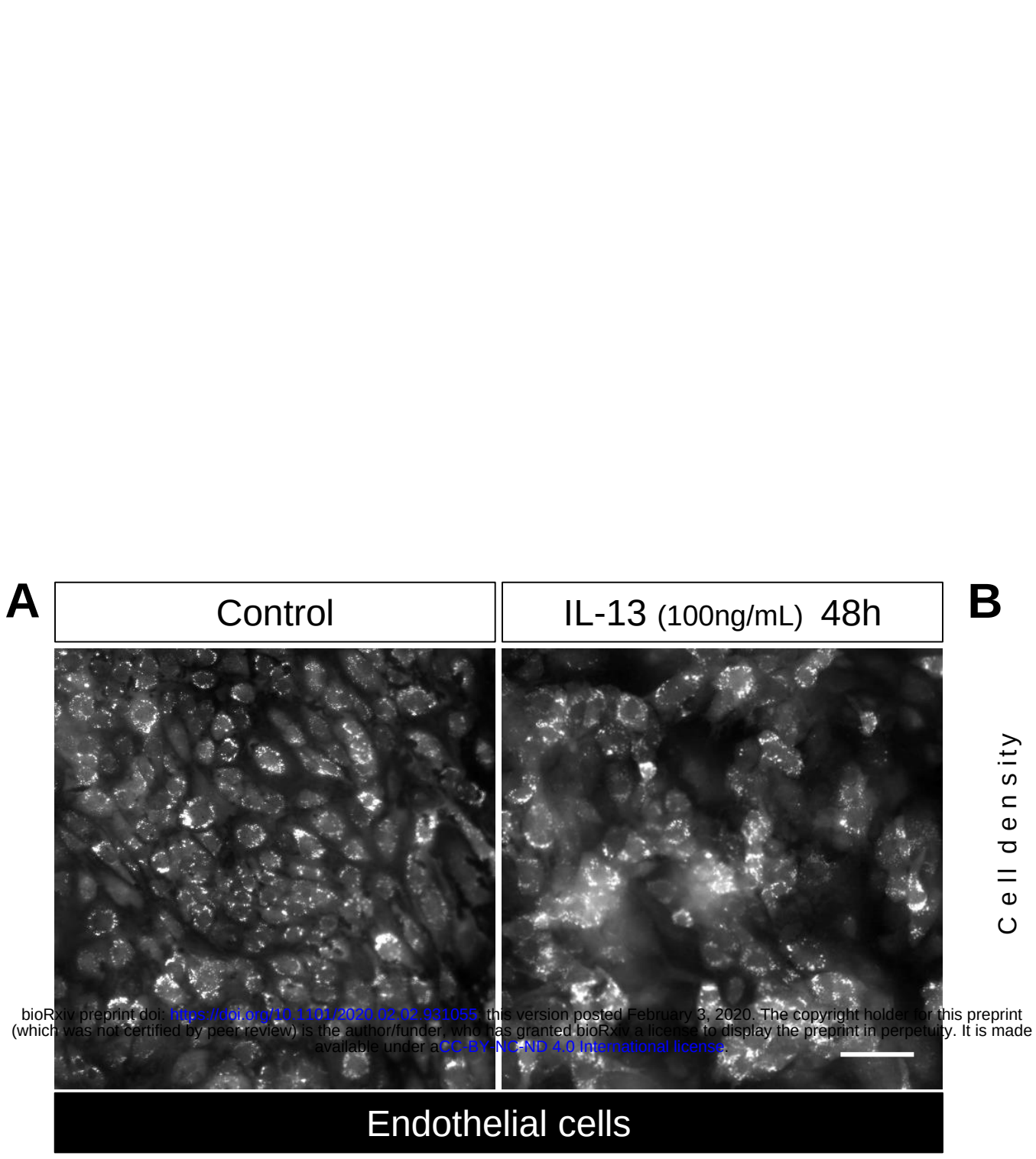

Fig 5. IL-13 induces aggregation and activation of endothelial cells. (**A**) Fluorescence micrographs of GFP-expressing endothelial cells co-cultured with well differentiated airway epithelial cells on chip, in absence (left) or presence (right) of IL-13 (100ng/mL) for 48h. Scale bar, 50 µm. (**B**) Quantification of endothelial cell density in absence or presence of IL-13 (100 ng/mL) for 48h. (**C**) Volcano plot showing gene expression of IL-13 (100ng/mL) treated endothelial cells compared to untreated group. Data were analyzed using a two-stage step-up method of Benjamini, Krieger and Yekutieli. (**D**) Effect of IL-13 (100ng/mL) on endothelial cell adhesion molecules ICAM-1 and VCAM-1 expression, as measured using fluorescence measurement. Data represent mean ±SEM of n=3 replicates. Significance was determined by unpaired Student's t-test; *P < 0.05, ****P < 0.0001.

FIGURE 5

Fig 6. Therapeutic modulation of IL-13- and HRV-induced neutrophil recruitment and infiltration with a CXCR2 antagonist on chip. (**A**) Schematic diagram of the severe asthma chip depicting the neutrophil recruitment assay. (**B**) Micrographs showing paracellular and transcellular transmigration of neutrophil live-stained (red) through GFP-expressing endothelial cells (green). Obvious transcellular diapedesis events are indicated by the pink arrows while the blue arrow points at a paracellular migration. Scale bar, 10 µm. (**C**) Fluorescence microscopic imaging of chips perfused through the microvascular channel under physiological conditions (shear stress, 1 dyn/cm^2) for 5 min with freshly isolated CellTracker red−labeled human neutrophils showing recruitment to the endothelium stimulated or not with a combination of IL-13, HRV-16 and a CXCR2 antagonist (MK-7123 - 10µM). Scale bar, 50 µm. (**D**) Quantification of neutrophil recruitment from (**C**). (**E**) Schematic diagram of neutrophil diapedesis taking place in the severe asthma chip. (**F**) Fluorescence imaging tracking neutrophil velocity at the endothelial surface in HRV-16 infected chips, in absence (left) or presence (right) of the CXCR2 antagonist. Scale shows color coded velocity values in µm/sec; Scale bar, 50 µm. (**G**) Quantification of neutrophil velocity in HRV16 infected chips with or without MK-7123 (10µM). (**H**) The graph shows real time cumulative quantification of disappearing neutrophil following transmigration from the vascular wall to the epithelial lumen in HRV16 infected chips in absence or presence of MK-7123 (10µM). (**I**) Immunofluorescence micrograph of an HRV16 infected chip showing human neutrophil stained for myeloperoxidase (green) that have migrated to the epithelial lumen among HRV16 infected epithelial cells (red). Scale bar, 20 µm. Data represent mean ± SEM from three different donors with two biological replicates (chips) per donor.

FIGURE 6

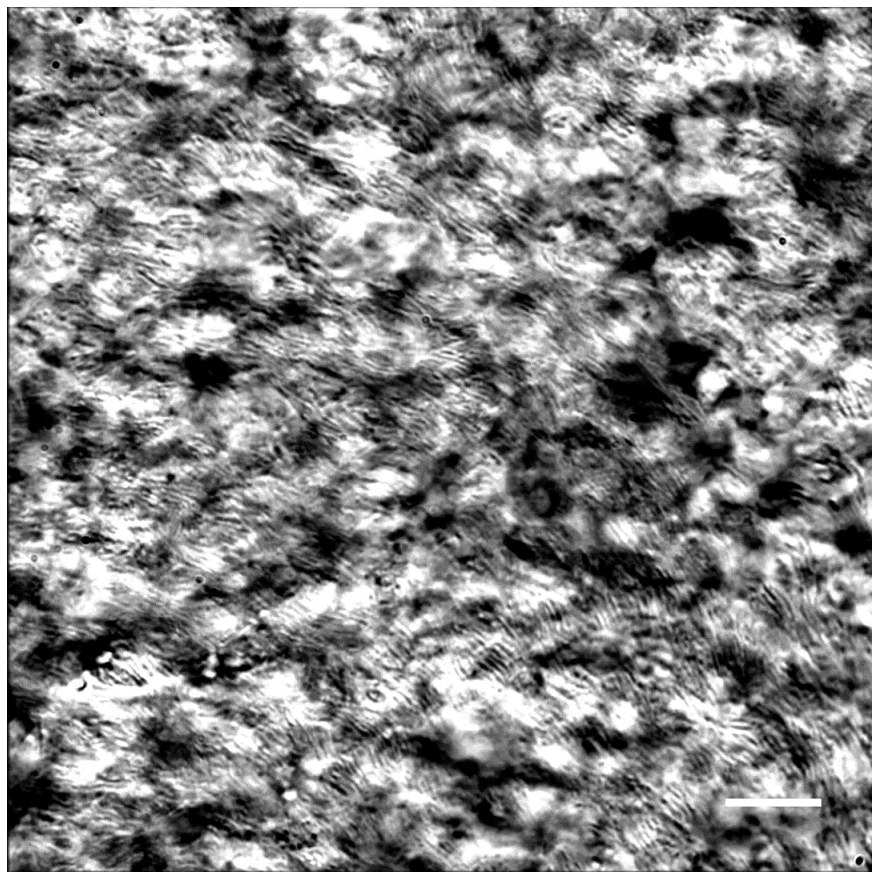

Supplementary movie 1. Real time phase contrast microscopic imaging of well differentiated human airway epithelial cells cultured inside the airway chip for 21 days on a 3 um pore membrane showing extensive coverage of synchronized cilia beating. Scale bar, 20 µm.

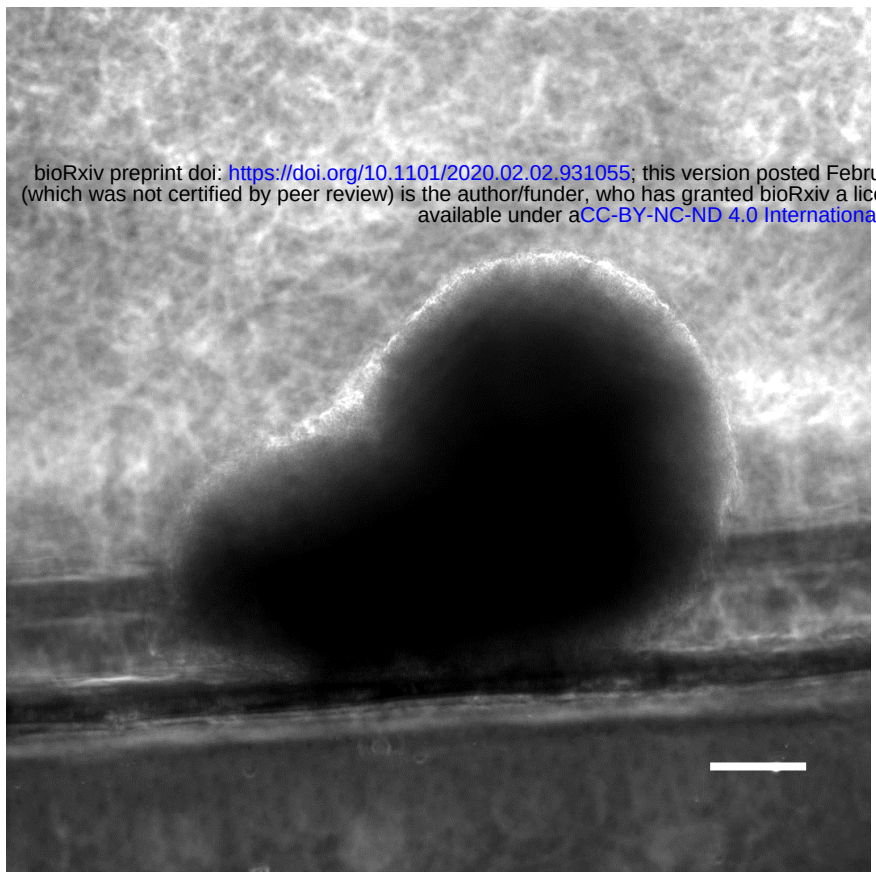

Supplementary movie 2. Real time phase contrast microscopic imaging of well differentiated human airway epithelial cells cultured inside the airway chip for 21 days on a 3 um pore membrane showing a mucus plug being displaced by active cilia beating. Scale bar, 50 µm.

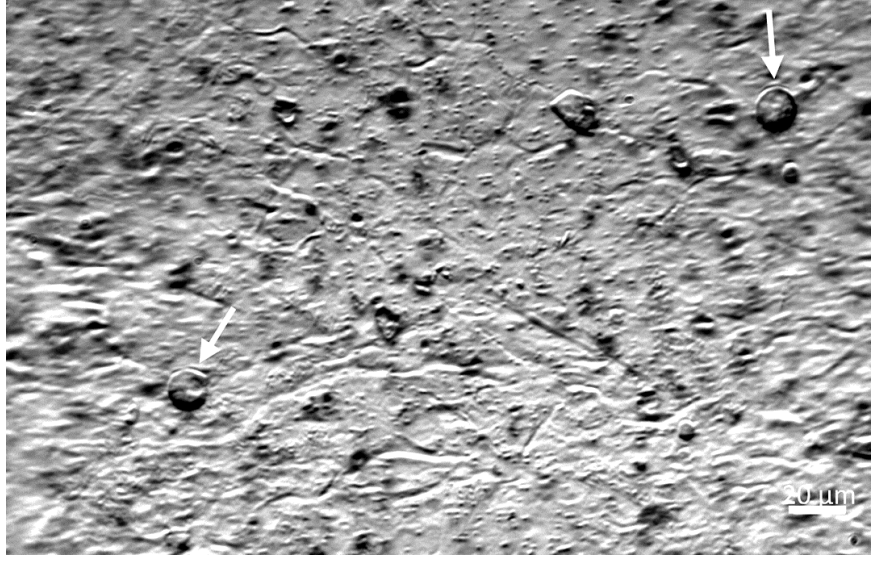

Supplementary movie 3. Real time phase contrast microscopic imaging of HRV16-infected airway chips (24hpi) showing rounded ciliated detaching from the epithelium (white arrows). Scale bar, 20 µm.

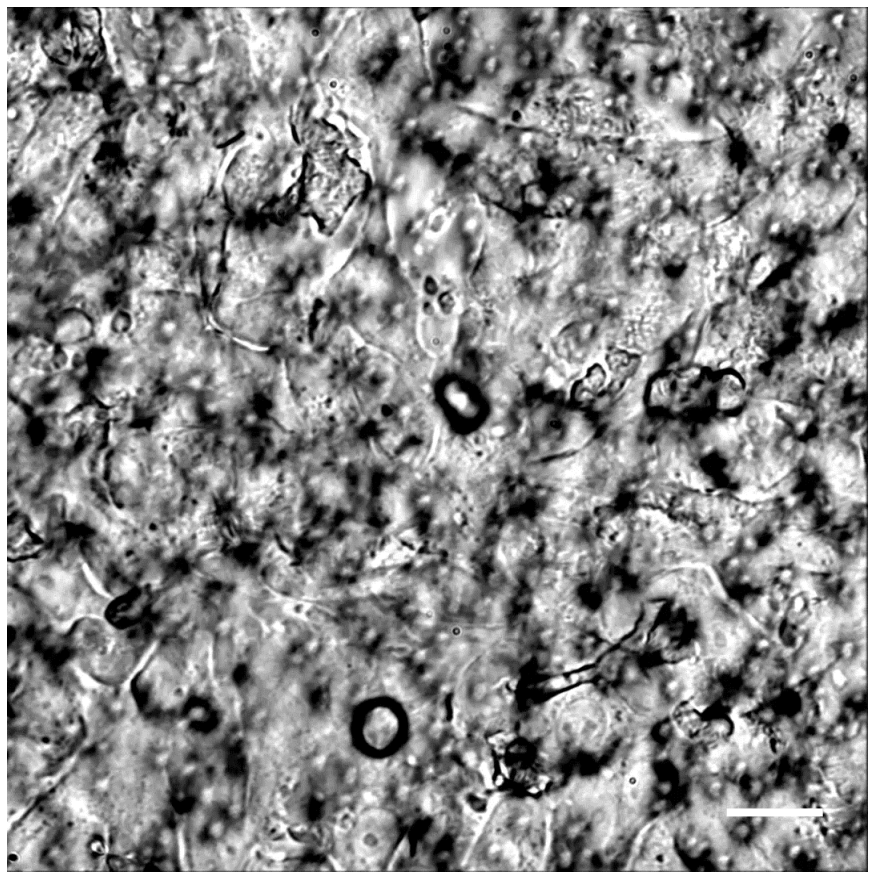

Supplementary movie 4. A movie showing phase contrast microscopic imaging of well differentiated human airway epithelial cells cultured inside the airway chip for 21 days on a 3 um pore membrane and infected with HRV16 for 72 h. Scale bar, 20 µm.

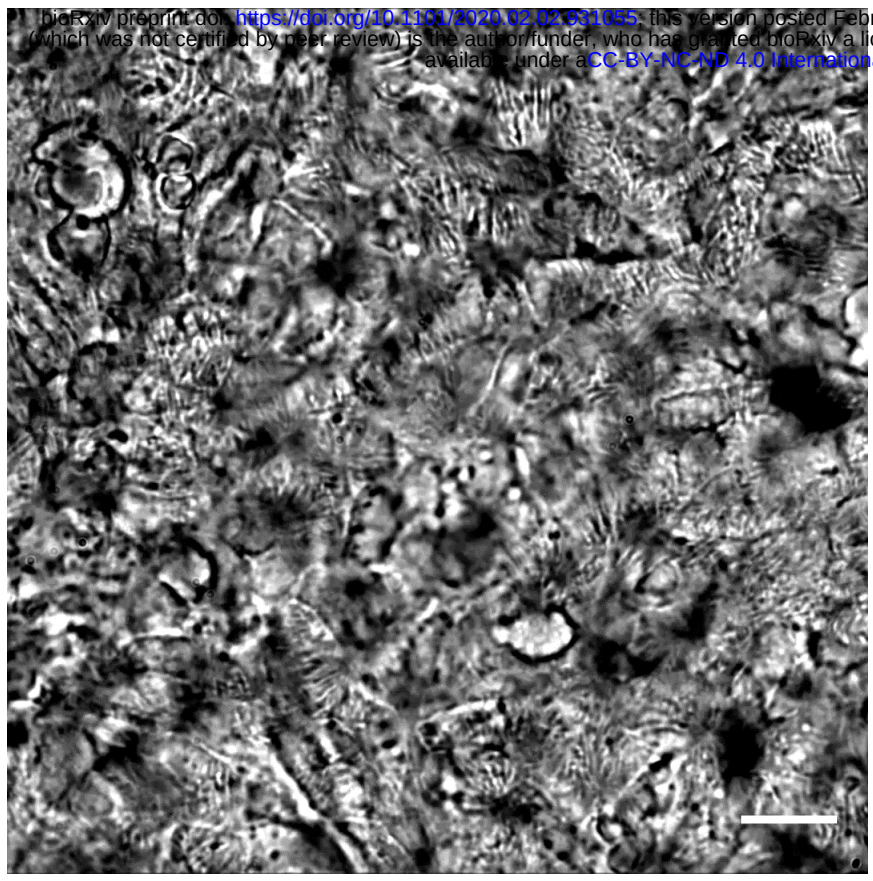

Supplementary movie 5. A movie showing phase contrast microscopic imaging of well differentiated human airway epithelial cells cultured inside the airway chip for 21 days on a 3 um pore membrane and treated with IL-13 (100 ng/mL) for 7 d. Scale bar, 20 µm.

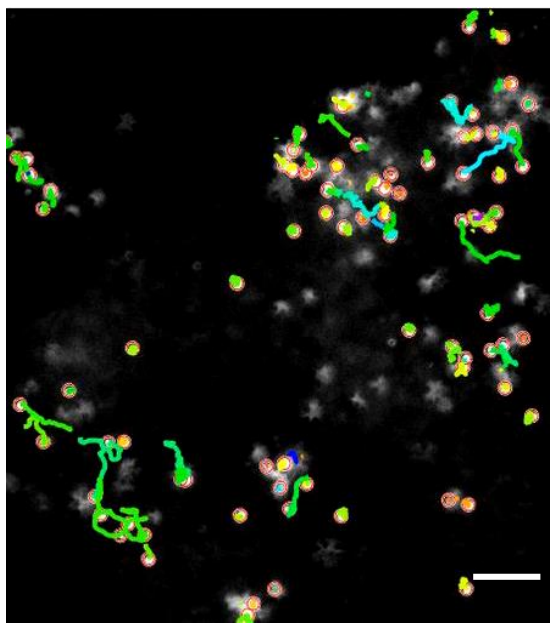

Supplementary movie 6. A movie showing movement tracking of fluorescently labelled human neutrophils recruited to the surface of the microvascular endothelium 24 post HRV16 infection on chip. Scale bar, 50 µm.

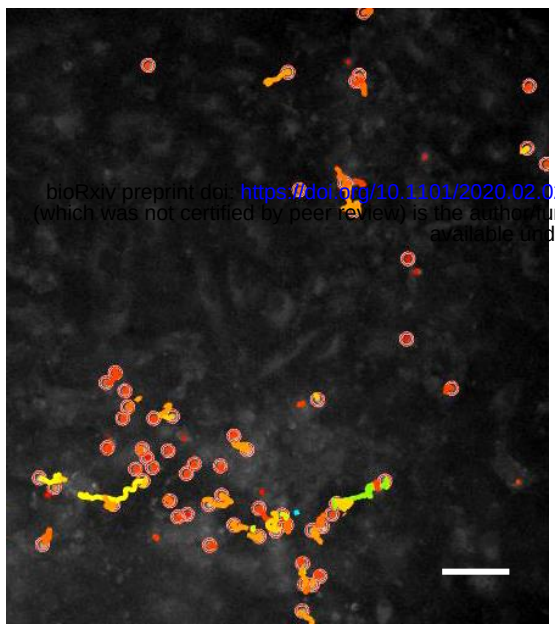

Supplementary movie 7. A movie showing movement tracking of fluorescently labelled human neutrophils recruited to the surface of the microvascular endothelium 24 post HRV16 infection and treated with the CXCR2 inhibitor, MK-7123 (10µM) on chip. Scale bar, 50 µm.

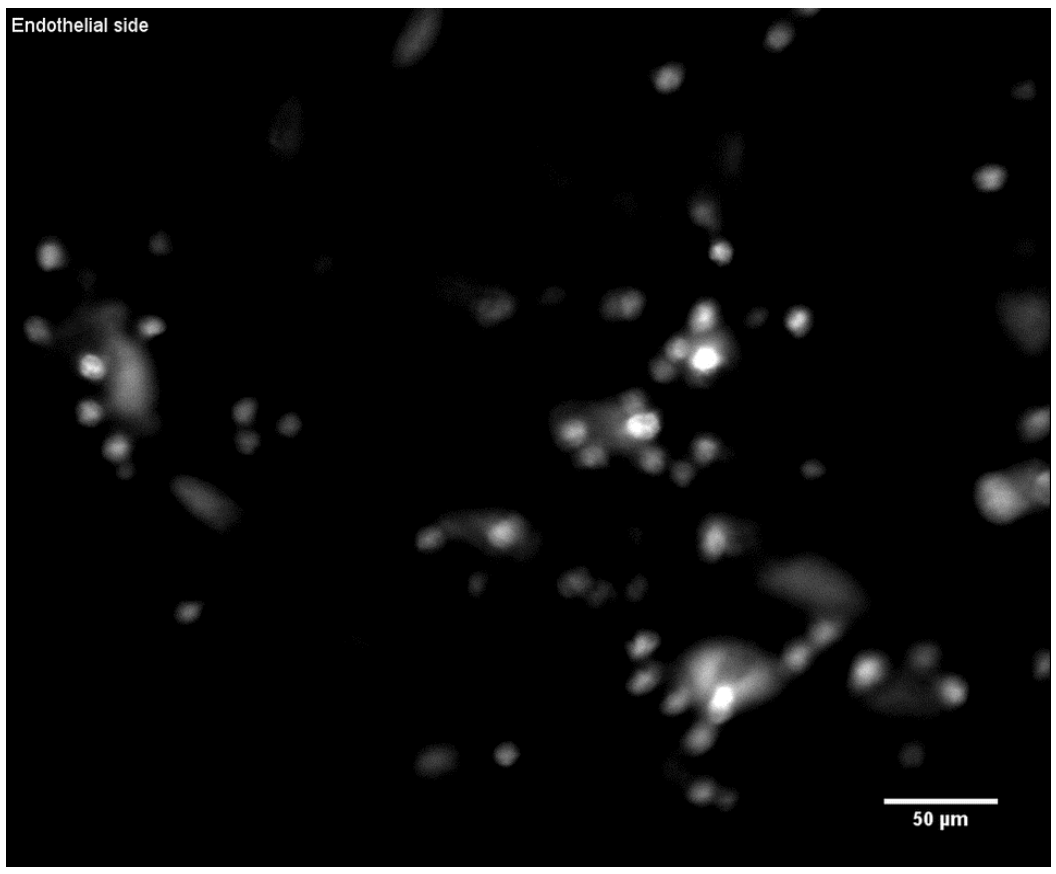

Supplementary movie 8. A movie of an orthogonal sectioning of a chip from the vascular to the epithelial compartment showing labelled neutrophil (white) at the surface of the microvascular endothelium and neutrophil that have crossed the membrane and transmigrated towards the epithelium. Scale bar, 50 µm.

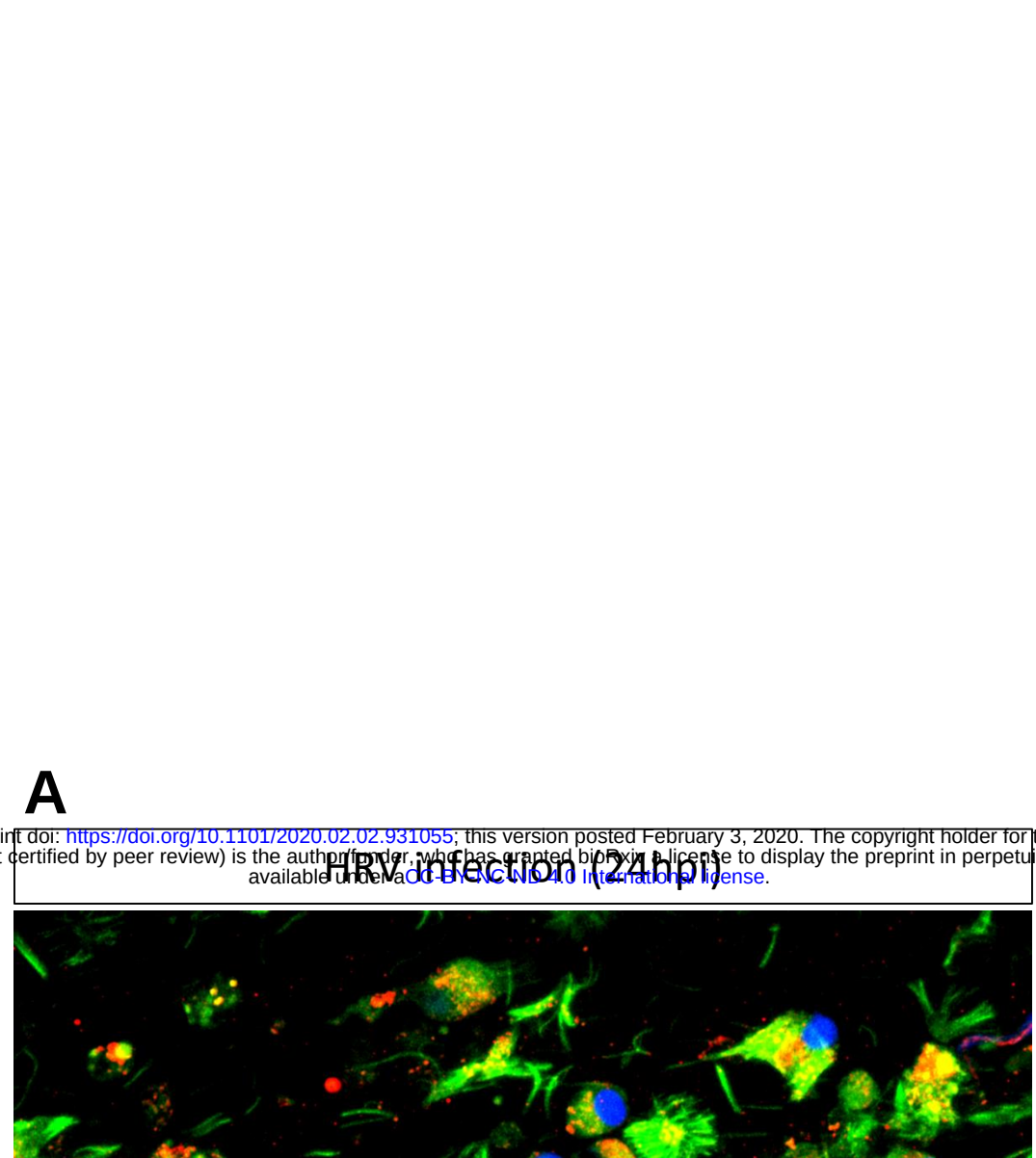

Supplementary figure 1. (A) Confocal image of the cells collected in an apical wash 24 h following HRV16 infection of an airway chip showing the extend of ciliated cells destruction. Note the presence of individual cilia (green) in the apical wash. Scale bar, 20 µm. (B) Quantification of the length of cilia on multiciliated cells 6 d post HRV16 infection. Data represent mean ± SEM; Significance was determined by unpaired Student's t-test; ****P < 0.0001.

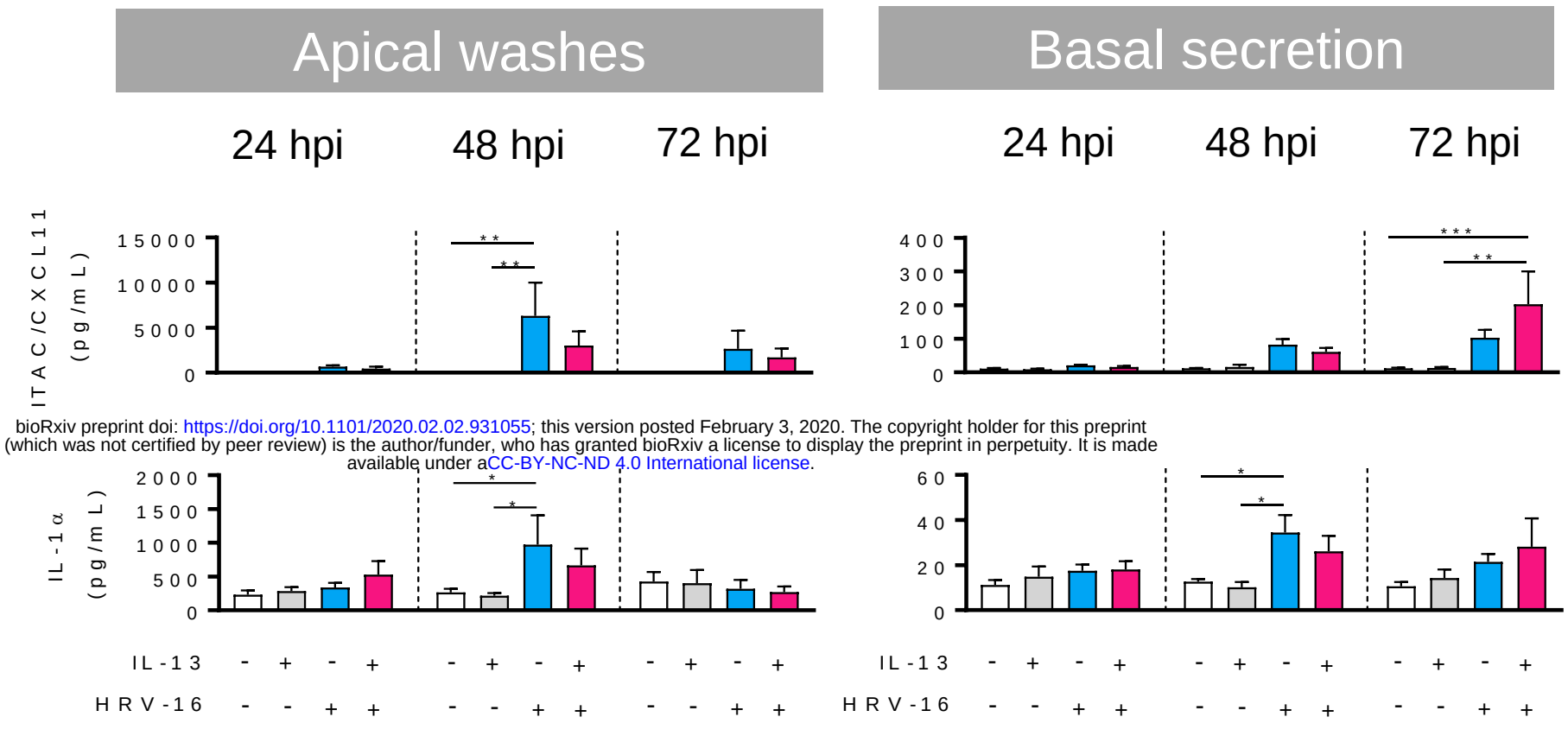

Supplementary figure 2. The graphs show the effect on polarized apical and basal release of CXCL11 and IL-1α by the combination of IL-13 treatment and HRV-16 infection in the severe asthma-on-a-chip at 24h, 48h and 72h post infection. Data represent mean ±SEM of cells from three to four different donors, with one or two biological replicates (chips) per donor. Significance was determined by multiple comparison two-way ANOVA followed by Tukey's post-hoc correction; *P < 0.05, **P < 0.01, ***P < 0.001.

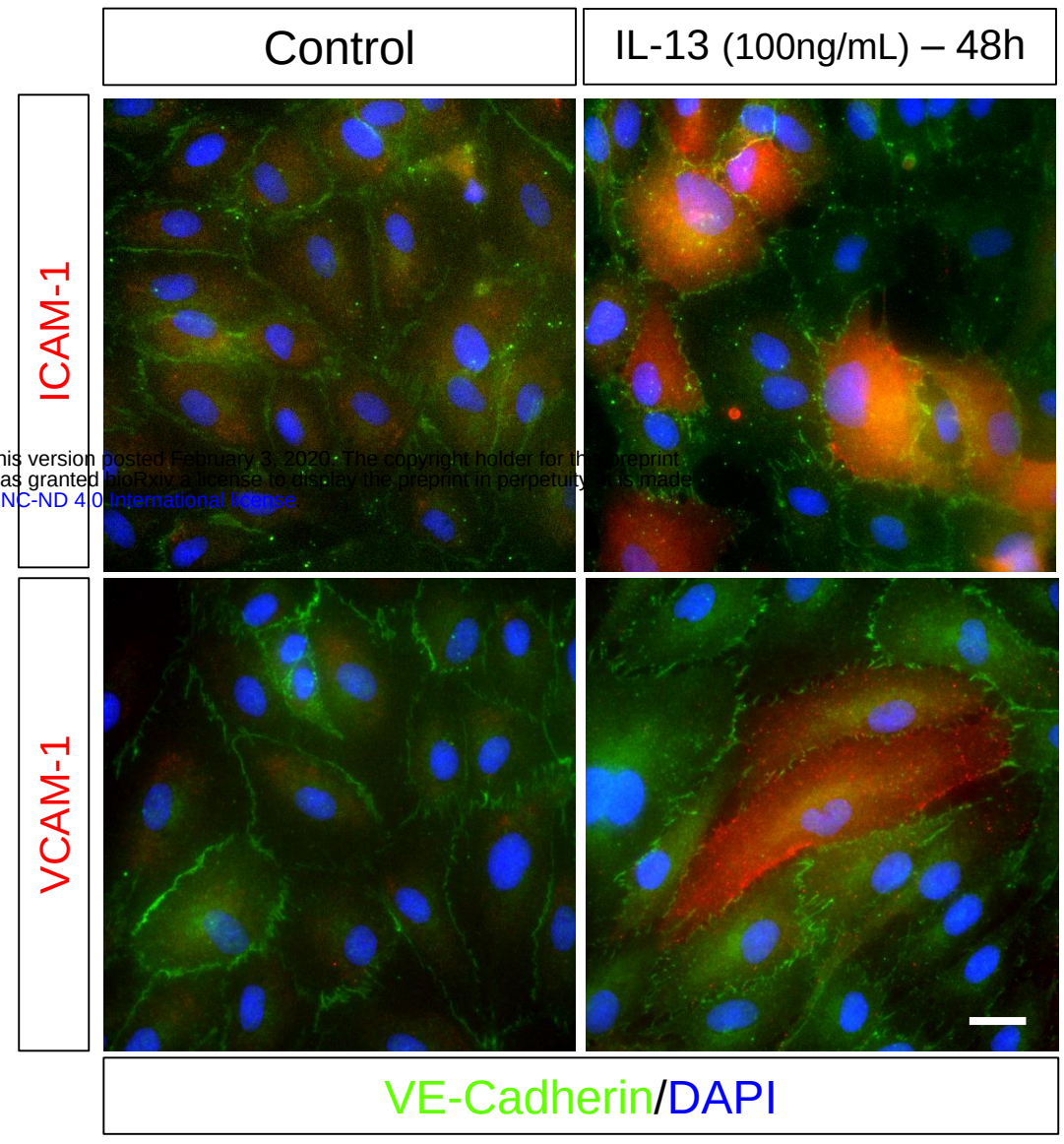

Supplementary figure 3. Fluorescent micrograph of human pulmonary microvascular endothelial cells in presence and absence of IL-13 (100 ng/mL) for 48h and stained for adhesion molecules ICAM-1 and VCAM-1 (red), and VE-Cadherin (green). Nuclei were counter stained with DAPI (blue). Scale bar, 20µm.

Donor #	AGE	SEX	SMOKING
1	5 yo	F	N
2	21 yo	M	N
3	18 yo	M	Y
4	18 yo	F	N

Supplementary table 1. Age and sex of donors used in this study.